26th Symposium on Naval Hydrodynamics
Rome, Italy, 17–22 September 2006

Large Eddy Simulation of Crashback in Marine Propellers

Martin Vyšohlíd, Krishnan Mahesh
(Aerospace Engineering & Mechanics, University of Minnesota)

ABSTRACT

The large eddy simulation methodology is used to predict and understand the unsteady flow around a marine propeller in crashback operation. A non-dissipative, robust numerical algorithm developed by Mahesh et al. (2004, J. Comput. Phys., 197: 215-240) for unstructured grids is extended to include the effect of rotating frame of reference. Flow around Propeller 4381 (for propeller specification see e.g. Jessup et al.: 2004, 25^{th} Symposium on Naval Hydrodynamics, 270–292) at advance ratio $J = -0.7$, Reynolds number $Re = 480,000$ (based on propeller diameter and relative speed between free-stream flow and the propeller) is computed for a period of 300 revolutions. The simulation shows the presence of a highly unsteady ring-vortex, and irregular low frequency unsteady loads on the propeller. The spectra also show distinct peak at higher frequency of 5 rev^{-1}, corresponding to passage of individual blades of the five-bladed propeller. Mean values, root mean square (RMS) fluctuations and spectra of computed thrust, torque and side-forces show good agreement with experiment. Circumferentially averaged mean velocity and RMS fluctuation of velocity obtained from the simulation are compared to experimental data and good agreement is observed. The cross-flow aft of the propeller, which represents inflow for a propeller in crashback, was investigated. The cross-flow shows low frequency fluctuations similar to spectra of side-forces, but without the peak at blade frequency of 5 rev^{-1}. An unsteady actuator disk model is constructed in order to understand unsteadiness in propeller crashback. The model considers crashback as a competition between two flows of opposite directions: reversed flow through the propeller and the ambient flow due to motion of the vessel. Visualization of the flow around the actuator disk in crashback shows creation, asymmetric growth, tilting, stretching and shedding of unsteady ring vortices which are correlated to the fluctuation of the thrust of the actuator disk.

INTRODUCTION

Crashback is an operating condition where the propeller rotates in the reverse direction while the vessel moves in the forward direction. Crashback is characterized by large scale unsteadiness and asymmetry of flow. This leads to significant low frequency fluctuations in propeller thrust, torque and side-forces, which affect maneuverability of the vessel. A prominent feature of the flow is an unsteady ring-vortex in the vicinity of the propeller disk. Jiang et al. (1997) performed experiments of propeller crashback which provide PIV data on the ring-vortex, and suggest that the unsteadiness of the ring-vortex is related to the forces experienced by the propeller. Detailed measurement of the flow velocity in crashback using PIV and LDV were recently published by Jessup et al. (2004).

The unsteady Reynolds-averaged Navier-Stokes equations (RANS) represent the state-of-the-art in computational prediction of the viscous flow around propellers (Chen & Stern, 1999; Davoudzadeh et al., 1997; McDonald & Whitfield, 1996). Currently, RANS appears capable of predicting forward mode and backing; however, significant disagreement with data is observed in crashback and crashahead conditions. For example, Chen & Stern (1999) show that RANS is within 5% of experimental data for thrust and torque in the forward mode and within 6.5% when backing, but crashback or crashahead increases the error to 110%. Also their computed results showed only 3% oscillation about the mean while the experiment showed 20%.

It is likely that RANS is unable to adequately predict crashback because of the pervasive large-scale unsteadiness. This paper therefore uses the large-eddy simulation (LES) methodology to simulate propeller crashback. The goal is to develop the LES capability for crashback prediction and to use this new method to achieve better understanding of the mechanism responsible for unsteady loads. Our previous results showed that LES can be used in the complex propeller geometry and good agreement for mean values of thrust and torque was obtained in forward mode (Vyšohlíd & Mahesh, 2005) as well as in crashback (2006), however only limited length of data in crashback was computed there. For this paper, simulations were extended for 300 propeller revolutions to capture low frequency behavior of

the flow. This allows us to estimate the power spectral density of thrust, torque, side-forces, cross-flow aft of propeller as well as to get more reliable statistics. The results are compared with the results of measurements of Jessup et al. (2004 and private communication). Furthermore, an unsteady actuator disk model of crashback is suggested and its results are discussed.

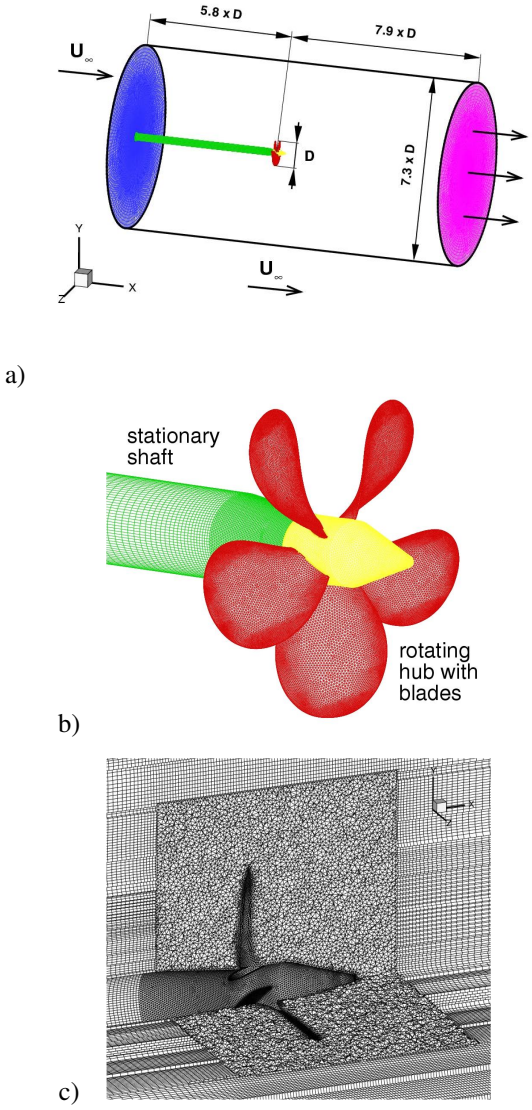

Figure 1: (a) Computational domain, (b) detail view of the propeller (c) mesh in propeller neighborhood.

PROPELLER SIMULATION DETAILS

Numerical Method

The simulations are performed in a frame of reference that rotates with the propeller. The incompressible Navier-Stokes equations are solved in a rotating coordinate system. The governing equations in a rotating frame can either be written for the velocities measured in a stationary frame or for velocities measured in the rotating frame. The form of the governing equations may be strongly conservative (Beddhu, 1996) or in a form where system rotation produces a source term (Majety, 2003). This paper uses the following form of the governing equations:

$$\frac{\partial u_i}{\partial t} + \frac{\partial}{\partial x_j}(u_i u_j - u_i \varepsilon_{jkl}\omega_k x_l) = -\frac{\partial p}{\partial x_i} - \varepsilon_{ijk}\omega_j u_k + \nu \frac{\partial^2 u_i}{\partial x_j \partial x_j}, \quad (1)$$

$$\frac{\partial u_i}{\partial x_i} = 0. \quad (2)$$

Here u_i is the inertial velocity, p is the pressure, x_i are coordinates in the rotating frame, t is time, ω is the angular velocity of the rotating frame of reference, and ν is the kinematic viscosity. Note that the density is absorbed in pressure. Also, the Einstein summation convention is used and ε_{ijk} denotes the permutation symbol.

The LES equations are obtained by spatially filtering (denoted by overbar) the Navier-Stokes equations. The filter is assumed to commute with the spatial and temporal derivatives. Applying the filter and using the approximation

$$\overline{u_i \varepsilon_{jkl} \omega_k x_l} \approx \bar{u}_i \varepsilon_{jkl} \omega_k x_l, \quad (3)$$

we get

$$\frac{\partial \bar{u}_i}{\partial t} + \frac{\partial}{\partial x_j}(\bar{u}_i \bar{u}_j - \bar{u}_i \varepsilon_{jkl}\omega_k x_l) = -\frac{\partial \bar{p}}{\partial x_i} - \varepsilon_{ijk}\omega_j \bar{u}_k + \nu \frac{\partial^2 \bar{u}_i}{\partial x_j \partial x_j} - \frac{\partial \tau_{ij}}{\partial x_j}, \quad (4)$$

$$\frac{\partial \bar{u}_i}{\partial x_i} = 0 \quad (5)$$

where

$$\tau_{ij} = \overline{u_i u_j} - \bar{u}_i \bar{u}_j \quad (6)$$

is the subgrid stress and is modeled. The dynamic Smagorinski model as proposed by Germano et al. (Germano, 1991) and modified by Lilly (Lilly, 1992) is used to model the subgrid stress.

The above equations are solved using a numerical method developed by Mahesh et al. (2004) for incompressible flows on unstructured grids. The algorithm is derived to be robust without numerical dissipation. It is a finite-volume approach which stores the Cartesian velocities and the pressure at the centroids of the cells (control volumes) and the face normal velocities are stored independently at the centroids of the faces. A predictor- corrector approach is used. The predicted velocities at the control volume centroids are first obtained

and then interpolated to obtain the face-normal velocities. The predicted face normal velocity is projected so that continuity is discretely satisfied. This yields a Poisson equation for pressure which is solved iteratively using a multigrid approach. The pressure field is used to update the Cartesian control volume velocities using a least-squares formulation. Time advancement is implicit and is performed using the Crank-Nicholson scheme. The algorithm has been validated for a variety of problems (Mahesh et al., 2004) over a range of Reynolds numbers.

Propeller Geometry and Grid

The computations were performed for a Propeller 4381, which is a five bladed, right-handed propeller with variable pitch, no skew and rake. The propeller diameter is 12 inches and a detailed description of the geometry may be found in Jessup et al. (2004). All five blades of the propeller are represented in the computation. The computational domain (see Figure 1) is a cylinder with diameter of 7.3 times the propeller diameter, and length of 13.75 times the propeller diameter. A constant free-stream velocity boundary condition is specified at the inlet and lateral boundaries. Convective velocity boundary conditions are prescribed at the outflow. The boundary condition on the propeller, hub and the conical tip are specified using $\vec{u} = \vec{\omega} \times \vec{r}$, while the shaft is stationary; i.e. $\vec{u} = 0$. A commercial grid generator (Gambit & TGrid, Fluent Corporation) was used for the grid generation. Tetrahedral elements are used in the immediate vicinity of the propeller to match the complicated geometry of the blades, while hexahedral elements and prisms are used farther from the propeller. Four layers of prisms were grown on the surfaces of blades in order to improve the resolution of boundary layers on blades. The smallest grid size is 1.7×10^{-3} of the propeller diameter, and is found on the edges of the blades; size functions were used to control the growth rate of the grid size to obtain a final mesh with size of approximately 13 million control volumes.

PROPELLER RESULTS

Simulations were performed under crashback conditions at advance ratio $J = -0.7$. The advance ratio J and Reynolds number Re are defined as

$$J = \frac{U}{nD}, \quad Re = \frac{DU}{\nu} \tag{7}$$

where U is the free-stream velocity, n is the propeller rotational speed in revolutions per time unit, D is the propeller diameter and ν is the kinematic viscosity.

The computation was started with a uniform flow as the initial condition with velocity equal to the free-stream velocity. The Reynolds number was $Re = 1,200$,

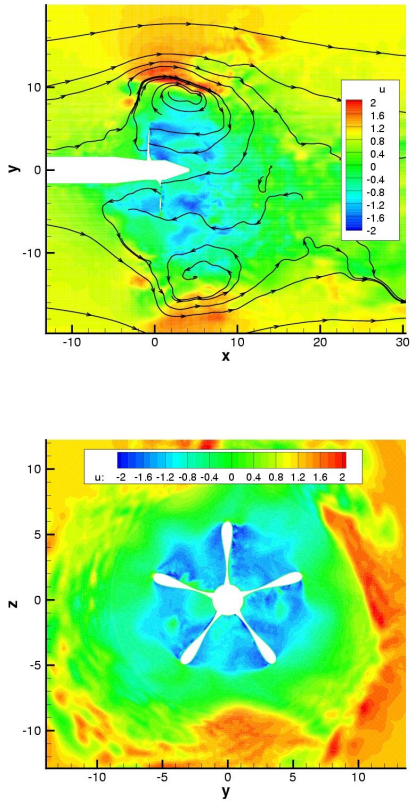

Figure 2: Contours of axial velocity normalized by free-stream velocity and streamlines for crashback $J = -0.7$, $Re = 480,000$: (a) side view (b) axial view at $x/D = 0$. contours correspond to axial velocity.

and 336 time steps per revolution were used. After 12 propeller revolutions, the Reynolds number was increased to $Re = 12,000$ and another 28 propeller revolutions were computed using 1680 time steps per revolution. Using the same time step, the Reynolds number was further increased to $Re = 120,000$ for 3 revolutions and then finally to $Re = 480,000$ for another 312 revolutions.

Note that the experiments of Jessup et al. (private communication) has shown that thrust does not depend on Reynolds number when $4 \times 10^5 < Re < 9 \times 10^5$. In the text, non-dimensional values of thrust K_T, torque K_Q and side forces K_{fy}, K_{fz} will be used.

$$K_T = \frac{T}{\rho n^2 D^4}, \quad K_Q = \frac{Q}{\rho n^2 D^5} \tag{8}$$

$$K_{fy} = \frac{F_y}{(\text{mean } T)}, \quad K_{fz} = \frac{F_z}{(\text{mean } T)} \tag{9}$$

where T is the propeller thrust, Q is the torque, ρ is the density, n is the propeller rotational speed in revo-

a) **Computed**

	K_T	K_Q	K_{fy}	K_{fz}
mean	-0.38	-0.072	0.004	-0.002
RMS	0.067	0.012	0.061	0.057

b) **Water Tunnel (Jessup)**

	K_T	K_Q	K_{fy}	K_{fz}
mean	-0.33	-0.065	0.019*	-0.006*
RMS	0.060*	0.011*	0.064*	0.068*

c) **Tow-Tank Data**

	K_T	K_Q
Jessup et al.	-0.41	-0.078
Hecker & Remmers	-0.50	0.093

Table 1: Mean value and RMS of non-dimensional propeller thrust K_T, torque K_Q and side forces K_{fy}, K_{fz} in crashback ($J = -0.7$): (a) our simulation, (b) water tunnel measurement of Jessup, (c) tow-tank measurement of Jessup and Hecker & Remmers. Values with a star symbol (*) were computed by authors using a record of 700 revolutions of data measured by Jessup. All experimental data, including Hecker & Remmers, were kindly provided by Jessup (private communication).

lutions per time unit, D is the propeller diameter and F_y, F_z are components of the force on propeller perpendicular to its axis. We assume that not only thrust, but also torque, side-forces and flow around propeller are similar in this range of Reynolds numbers, so that comparison with available experimental data can be made.

Ring Vortex in Crashback

The flow in crashback is complex and unsteady. Consider an example of instantaneous flow obtained from the computation. Figure 2a) shows streamlines and axial velocity contours in a plane along the propeller axis. There is a region of reversed flow close to the propeller in crashback (the blue and green region). This reversed flow interacts with ambient flow and creates a recirculation zone, which is often called a ring vortex. Figure 2b) shows axial velocity contours in a plane perpendicular to the axis of propeller. This illustrates asymmetry of the solution in the various blade passages.

Time History of Loads

The computed evolution of thrust K_T and torque K_Q is shown in Figures 3a) and 3b), respectively. The horizontal straight lines in figures show mean values measured in three different experiments. Both thrust and torque show large amplitude low-frequency fluctuations

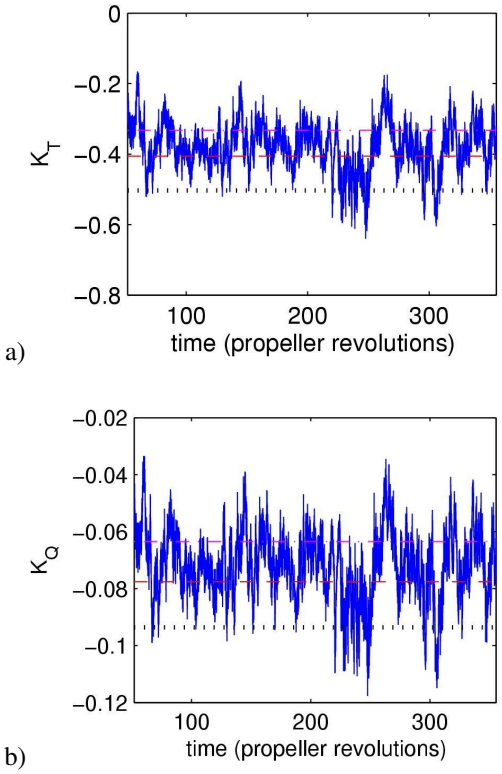

Figure 3: The blue continuous lines shows fluctuations of non-dimensional a) thrust K_T and b) torque K_Q as they change in time. The dotted (black), dashed (red) and dash-dotted (purple) straight lines show mean values measured in a tow-tank by Hecker & Remmers, in a tow-tank by Jessup and in a water tunnel by Jessup, respectively.

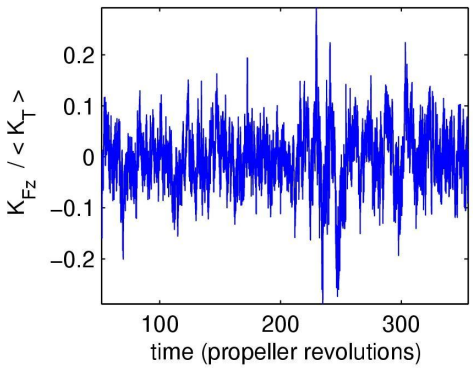

Figure 4: Fluctuations of a z-axis component of side-force K_{fz} (blue continuous line) as function of time in propeller revolutions.

around the experimental mean values. Comparison of the Figures 3a) and 3b) shows strong correlation between propeller thrust and torque. Figure 4 shows the evolution of a component of the side-force, K_{fz}. The side-forces show large amplitude low-frequency oscillations around zero. Thrust and torque appear to have lower frequency than that of the side-force.

Mean Values and RMS Fluctuations of Loads

Table 1 compares computed mean values and RMS fluctuations of propeller thrust K_T, torque K_Q and side-forces K_{fy}, K_{fz} with experiment. K_{fy}, K_{fz} are side-forces in two perpendicular directions – their mean values should ideally be zero and their RMS should be equal, but note that in practice they are slightly different, which gives some idea about uncertainty in both measurement and computation.

The results in Table 1a) were computed from last 300 revolutions. The results in Table 1b) are from a water tunnel measurement of Jessup (2004 and private communication) and results in Table 1c) are from a tow-tank measurements of Jessup (private communication) and Hecker & Remmers (1971). The computed results show reasonable agreement with experiment.

Power Spectral Density of Loads

Figure 5 shows the power spectral density of thrust from simulation of 300 propeller revolutions and from experimental data (700 revolutions of data obtained from Jessup). Note the high spectral density at the lowest frequency. The spectra show very good agreement in the middle part and both show peak with frequency 5 rev^{-1} which corresponds to passage of individual blades of five bladed propeller. In addition, the experimental data show multiple lobes near the 5 rev^{-1} frequency and other higher frequency peaks (12-18 rev^{-1}) that are not present in the spectrum from simulation. According to Jessup (private communication) the differences at high frequency part of spectrum could be due to blade bending or blade vibration, or other shaft related resonances effecting the measured data. Similar agreement is obtained for power spectral density of torque.

Figure 6 shows the power spectral density of non-dimensional side-force from simulation and from experimental data. The agreement is very good except at the very highest frequency (similar as for thrust), and discrete frequency peaks at 1 rev^{-1} and its harmonics that appear in experimental data. The maximum of power spectra density of side-force is achieved at higher frequency than in the case of thrust.

Circumferentially Averaged Flow

The computed results were averaged circumferentially and in time over a period of 300 revolutions and

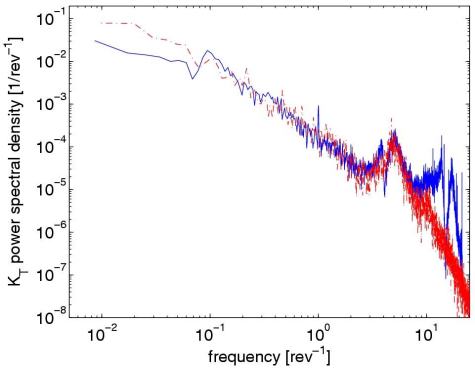

Figure 5: Power spectral density K_T of non-dimensional thrust. Red dash-dotted line is computed, blue line is from experiment.

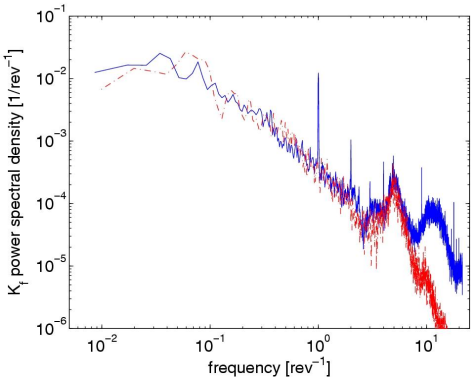

Figure 6: Power spectral density K_f of a component of non-dimensional side-force. Red dash-dotted line is computed, blue line is from experiment.

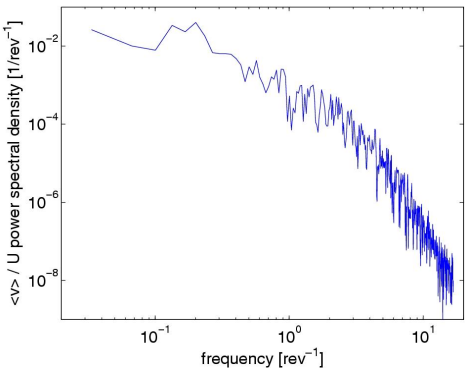

Figure 7: Power spectral density $<v>/U$ of a component of cross-flow at crashback inflow averaged over disk of propeller radius R at $x/R = 0.23$ and non-dimensionalized by free-stream velocity.

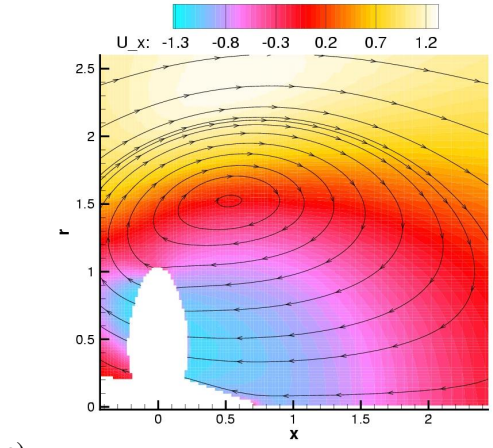

a)

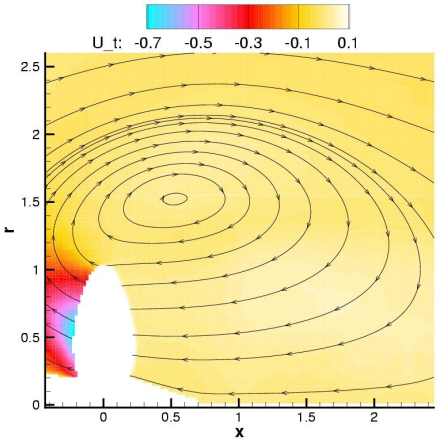

b)

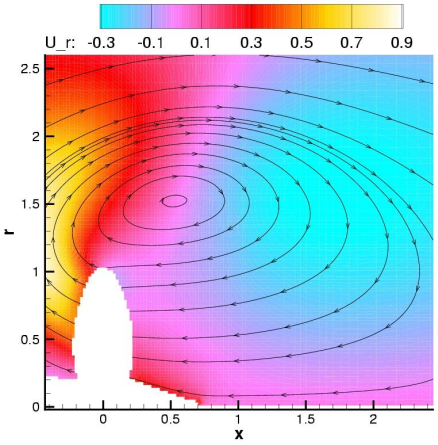

c)

Figure 8: Computed velocity and streamlines averaged circumferentially and in time over 300 propeller revolutions (normalized by free-stream velocity) for crashback $J = -0.7$, $Re = 480,000$: (a) axial velocity, (b) tangential velocity, (c) radial velocity.

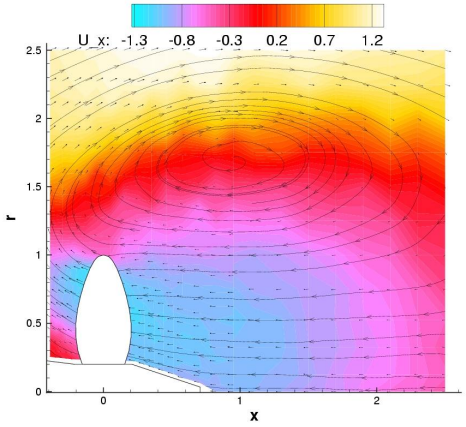

a)

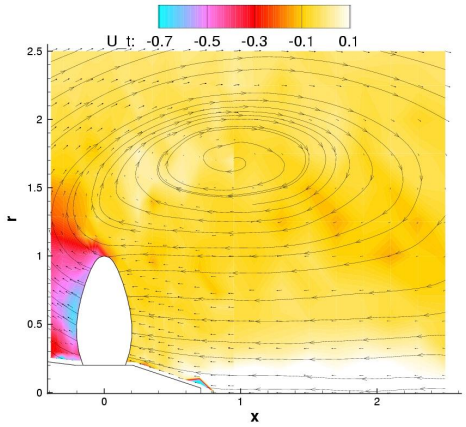

b)

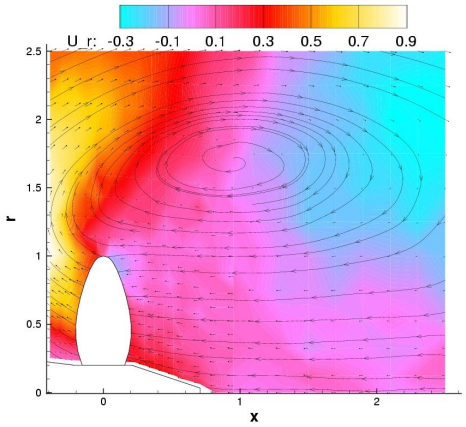

c)

Figure 9: Velocity and streamlines averaged circumferentially and in time (normalized by free-stream velocity) for crashback $J = -0.7$, $Re = 650,000$ measured by Jessup at al.: (a) axial velocity, (b) tangential velocity, (c) radial velocity.

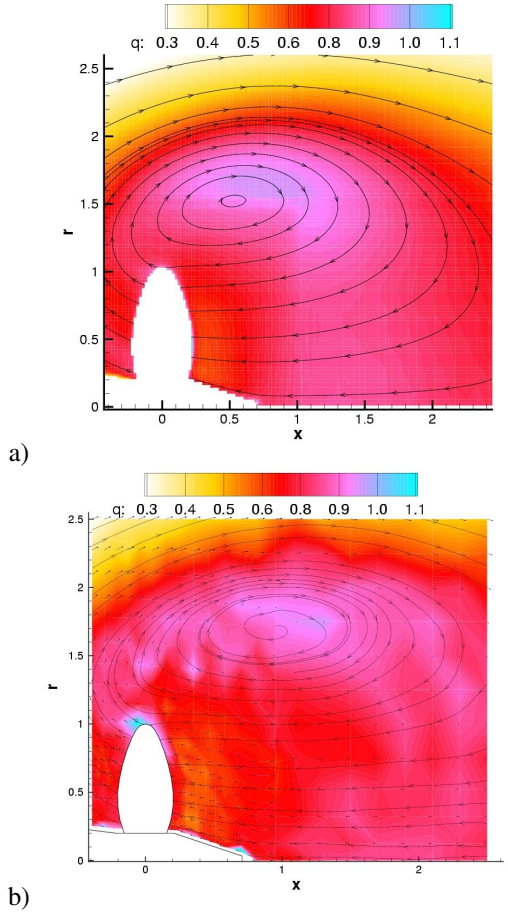

Figure 10: Root-mean-square fluctuation of velocity averaged circumferentially and in time (normalized by free-stream velocity) for crashback $J = -0.7$: (a) computed over 300 propeller revolutions at $Re = 480,000$, (b) measured by Jessup at al. in water tunnel at $Re = 650,000$.

compared with corresponding experiment. Figure 8 shows computed velocity, Figure 9 shows experimental result of Jessup (2004). Figure 8a) shows contours of computed axial velocity and streamlines, Figure 9a) shows experimental result. Note the reversed flow through the region where propeller blades operate. This reversed flow interacts with surrounding flow to create a ring vortex. The computed ring vortex is somewhat closer to the propeller than the ring vortex observed in experiment, but the computed axial velocity is in a good agreement with experiment. Figures 8b) and 9b) compare computed and measured velocity in the circumferential direction (the propeller rotates in negative circumferential direction). The computed and measured data show very good agreement upstream from propeller (upstream with respect to free-stream flow), but downstream of the propeller, where the circumferential velocity is smaller, the agreement is weaker. The recirculation zone might require higher resolution to get better agreement of circumferential velocity downstream, but as its amplitude is small, it probably would not effect prediction of propeller performance. The radial component of velocity in Figures 8c) and 9c) shows very good agreement upstream of propeller. The computed radial velocity downstream of propeller drops faster than the measured radial velocity, which is consistent with location of the computed ring vortex slightly upstream of the ring vortex in experiment. Figures 10 a) and b) compare RMS fluctuation of velocity with experiment. Note that only resolved motions, not subgrid-scale fluctuations in LES are considered when RMS fluctuation of velocity is computed. Both graphs show high RMS fluctuation velocity in ring vortex region. A good agreement is achieved except in a small region near the tip of blade where experiment shows high RMS fluctuation velocity, but only small value is predicted. Overall, the circumferentially averaged velocity and RMS show encouraging agreement.

Explanation for Loads

The flow in crashback is highly unsteady as is documented in Figure 11, which shows pressure contours (normalized by square of free-stream velocity) and streamlines at two different times. As can be seen from the streamlines, an unsteady ring vortex is formed as observed in experiments by Jiang (1997). The ring vortex moves upstream and downstream and it tilts, which affects the flow near the propeller and hence also the thrust, torque and side-forces. Figure 11a) corresponds to higher absolute value of thrust whereas Figure 11b) corresponds to lower absolute value of thrust. This difference in thrust is obvious from the pressure contours – Figure 11a) shows higher pressure drop across the blades than Figure 11b). Also note that in crashback the sign of the pressure difference on the blades is such as to push the propeller in direction of the free-stream flow, i.e. to reduce the relative velocity between free-stream flow and the vessel.

It is expected that side forces would be related to flow aft of the propeller, which is upstream of propeller with respect to reversed flow through the propeller or simply inflow. Figure 12 shows cross-flow in plane $x/R = 0.23$ using streamlines and contours of velocity. The flow is very unsteady and asymmetric. The crashback inflow velocity was averaged over a disk with propeller diameter R at $x/R = 0.23$ (shown as a dashed line circle in Figure 12). Time evolution of the disk averaged inflow was computed for interval of 30 revolutions and a power spectral density of a cross-flow component was plotted in Figure 7. Note that the peak at 5 rev^{-1} is not

present. Spectrum shows maximum at frequency ≈ 0.2 rev^{-1}, which is higher than that of side-forces in Figure 4, however the length of inflow data of 30 propeller revolution is too short to perform this comparison. In fact, when segments of the same length were taken from side-force data, either computed or from experiment, it was found that some segments also show spectra with peak frequency of ≈ 0.2 rev^{-1}, while other show much lower frequency.

UNSTEADY ACTUATOR DISK

The unsteadiness in propeller crashback may be considered to originate from two different sources: 1) the competition between two flows of opposite directions – the reverse flow through the propeller and the ambient flow due to the motion of the vessel, and 2) the fact that the propeller operates in the local unsteady flow in reverse, which means that the roles of leading and trailing edges of each blade are reversed – the local flow sees the sharp edge as leading edge and the thicker edge as trailing edge. The aim of the unsteady actuator disk model is to understand the role of the first source of unsteadiness: the competition between two flows of opposite directions.

Model Description

Figure 13 shows a schematic of the actuator disk model. The propeller is approximated by a thin actuator disk with the same diameter as the real propeller which enforces constant velocity of flow through the disk: axial component equals U_P and lateral components are zero (swirl motion is neglected here). Beside this approximation, everything is the same as in the real propeller problem described earlier in this paper: The incompressible Navier-Stokes equations are solved; the domain of solution is a cylinder minus the actuator disk. Boundary conditions are: constant velocity U_P on the surface of the actuator disk (internal boundary), a constant free-stream velocity U at the inlet and lateral boundaries, and convective velocity boundary condition at the outflow. Thrust T can be obtained as the force of fluid acting on the actuator disk surface. In order to model a real propeller, the disk velocity U_P needs to be set to the average value of axial velocity through the real propeller. Non-dimensional thrust K_T can be obtained using Equation 8 where n would be the rotational speed of the corresponding real propeller.

Note that there is no distinction between forward operation and backing, and no distinction between crashback and crashahead in this model. Actuator disk approximations have been used earlier as a simplified model of forward propeller operation by Rankine and Froude (Carlton, 1994). However, in their theory addi-

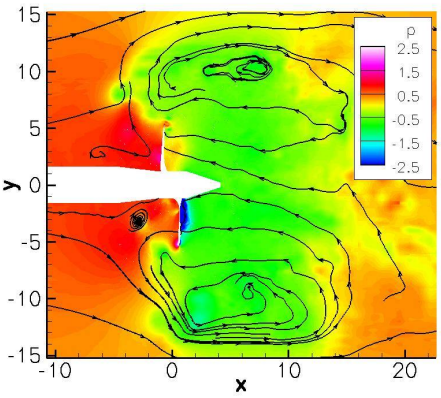

a)

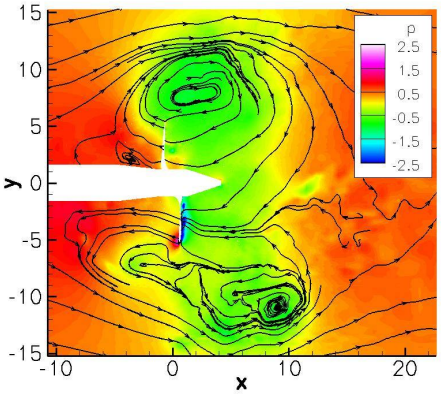

b)

Figure 11: Contours of pressure normalized by ρU^2 and streamlines for crashback $J = -0.7$, $Re = 480{,}000$ at two different times corresponding to: (a) high thrust, (b) low thrust.

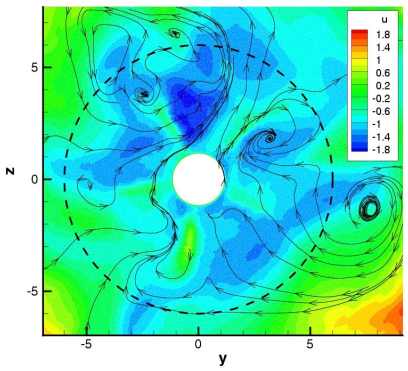

Figure 12: Cross-section $x/R = 0.23$: streamlines show cross-flow, contours correspond to axial velocity normalized by free-stream velocity.

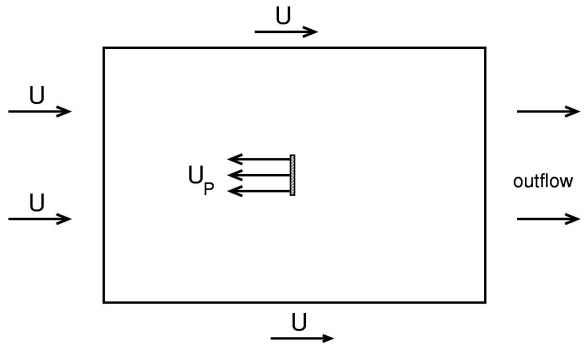

Figure 13: Schematics of unsteady actuator disk model.

tional assumptions were made about the flow, here we only make the disk approximation of the propeller; we solve the three-dimensional, viscous, unsteady Navier-Stokes equations.

Modes of Operation

Streamlines and contours of axial velocity for four different values of parameter U_P/U computed at low Reynolds number $Re = 100$ are in Figure 14. $U_P/U = 2$ in Figure 14a) corresponds to forward operation of propeller. The flow accelerates as it passes through the disk and the solution looks similar to that of jet in a strong co-flow. Figure 14b) shows the solution for $U_P/U = 0.5$. Here the flow decelerates as it passes through the disk. There is a region of slightly accelerated flow around the disk as the decrease of velocity through the disk creates a constraint, but the flow still remains without large re-circulation zones. This changes in Figure 14c), which shows solution for $U_P/U = 0$ where the disk acts as a bluff body with irregular recirculation zones downstream of the disk. Still in all cases in Figures 14a), 14b) and 14c) the fluctuation of thrust is small.

Figure 14d) shows solution for $U_P/U = -1$. In this case a recirculation zone in shape of a ring vortex is created which significantly influences the flow both downstream and upstream of the disk. In this case the fluctuation of thrust is much larger, similar as in the case of propeller crashback. The parameter $U_P/U = -1$ was chosen so that the flow through the disk resembles the flow around real Propeller 4381 at advance ratio $J = -0.7$. Notice that the reverse flow through the propeller and the ring vortex in Figure 2 are similar to the actuator disk result in Figure 14d).

Ring Vortex and Thrust in Crashback

The crashback mode ($U_P = -1$, $Re = 1200$) of unsteady disk actuator was further investigated to observe behavior of the ring vortex and its relation to the fluctu-

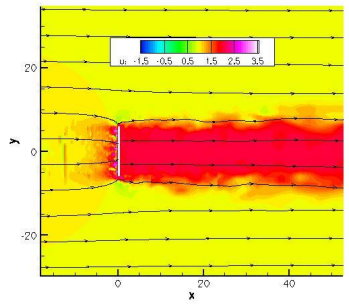

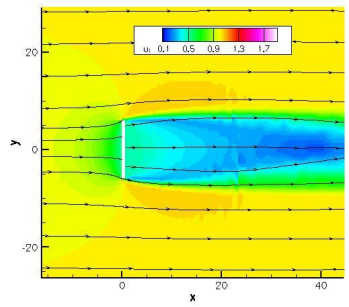

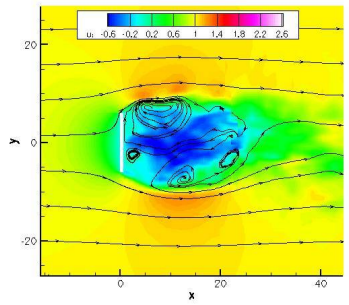

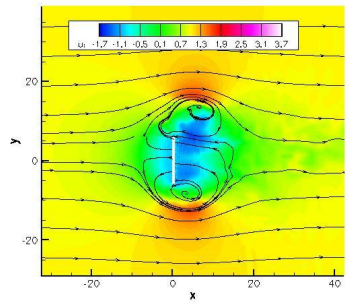

Figure 14: Axial velocity contours and streamlines for unsteady actuator disk model.(a) $U_P/U = 2$, (b) $U_P/U = 0.5$, (c) $U_P/U = 0$, (d) $U_P/U = -1$.

ations of thrust. The ring vortex was visualized in three dimensions by plotting the regions of low pressure.

Figure 15 shows evolution of the ring vortices in time. Contours of axial velocity are plotted on surfaces corresponding to a small constant pressure. Note that the axial velocity inside the ring vortices is negative – opposite to free-stream – while the axial velocity outside of the rings is positive and larger than free-stream. This illustrates the flow circulation in ring vortices.

Changes in position, strength and shape of ring vortices affect the flow in the neighborhood of the propeller and therefore also the thrust. Non-dimensional thrust is plotted in Figure 16. The narrow peaks of thrust (i.e. narrow local minima of thrust magnitude, because thrust is negative) correspond to shedding of ring vortices. Arrows marked a), b), c) and d) show thrust values at times corresponding to Figures 15a), 15b), 15c), 15d), respectively. Figure 15a) shows a new ring vortex (right) created around the actuator disk (not shown) while the old ring vortex (left) drifts away with the free-stream flow (from right top to left bottom corner) combined with the ring vortex self-induced velocity. The magnitude of thrust is maximal at this time. Then it drops as the ring vortex develops and then slowly increases again as the ring vortex grows and gets further from the actuator disk as in Figure 15b). After it grows larger it starts stretching with one point attached close to the actuator disk as in Figure 15c) which corresponds to local maximum of thrust magnitude. Finally, the ring detaches as in Figure 15d) which corresponds to the narrow local minimum of thrust magnitude and the irregular cycle starts again.

It is encouraging to see similarities between the simplified unsteady actuator disk model and the real propeller. Future work will further examine the relationship between the actuator disk model and the real propeller.

CONCLUSIONS

LES was applied to the turbulent flow around a marine propeller in crashback operation. Mean values, RMS fluctuations and spectra of thrust, torque and side-forces are in a good agreement with experiment. The simulation shows the presence of unsteady ring vortex and low frequency unsteadiness in thrust, torque and side-forces on propeller. Circumferentially averaged mean velocities and RMS of velocity fluctuation also show reasonable agreement with experiments.

An unsteady actuator disk model was proposed and investigated. Modes similar to forward and crashback operation were observed. Crashback mode of the disk model shows low frequency fluctuations of thrust and unsteady ring vortex similar to crashback mode of the real propeller. Fluctuations of thrust in the disk model

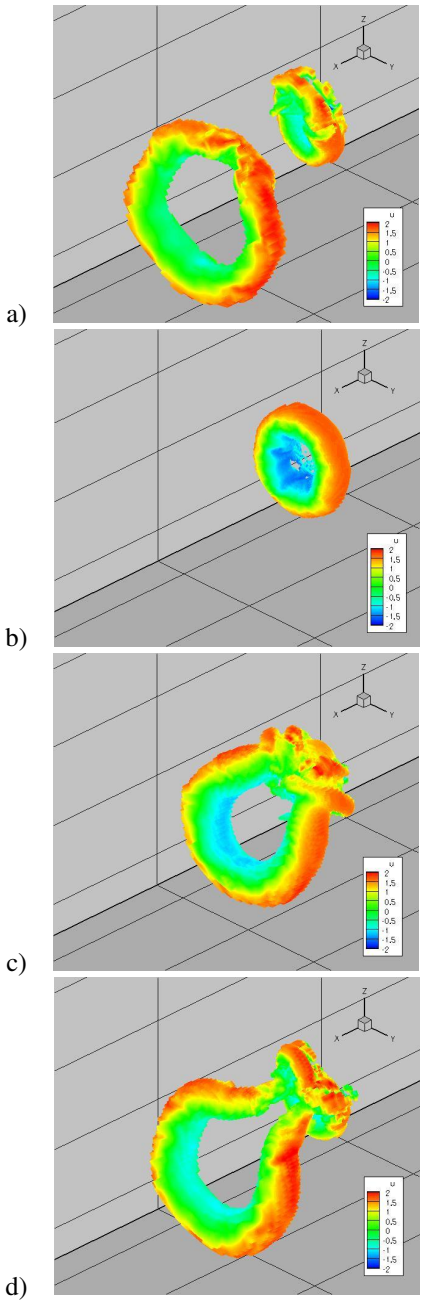

Figure 15: Time evolution of the ring vortex for actuator disk with $U_P/U = -1$, $Re = 1200$. Colors show axial velocity at an iso-surface of low pressure in a 3-D view. Free-stream flow is in positive x-direction, i.e. from right top to left bottom corner; the actuator disk is not plotted. In sequence: (a) shows a new ring vortex (right) created around the actuator disk while the old ring vortex (left) drifts away, (b) shows growth of the ring vortex, (c) ring vortex is stretched downstream, (d) ring vortex is shed, while a new one appears.

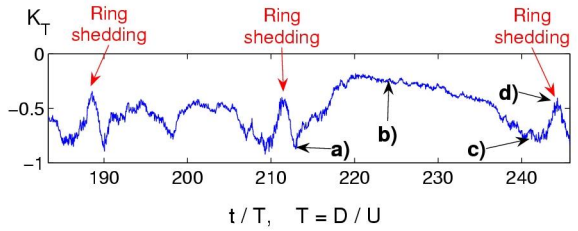

Figure 16: Time evolution of thrust in unsteady actuator disk model. Arrows marked a), b), c) and d) correspond to time instances in Figures 15a), 15b), 15c) and 15d), respectively.

are clearly correlated to creation, asymmetric growth, tilting, stretching and shedding of ring vortices.

ACKNOWLEDGEMENTS

This work was supported by the United States Office of Naval Research under ONR Grant N00014-02-1-0978 with Dr. Ki-Han Kim as technical monitor. Computing resources were provided by the San Diego Supercomputing Center, the National Center for Supercomputing Applications, and the Minnesota Supercomputing Institute. We are grateful to Dr. Stuart Jessup for providing us with experimental data, and for useful discussions.

REFERENCES

Jiang, C.-W., Dong, R. R., Liu, H.-L., Chang, M.-S., "24-inch Water Tunnel Flow Field Measurements During Propeller Crashback," 21st Symposium on Naval Hydrodynamics, The National Academies Press, Washington, DC, 1997, pp. 136–146.

Jessup, S., Chesnakas, C., Fry, D., Donnelly, M., Black, S., Park, J., "Propeller Performance at Extreme off Design Conditions," 25th Symposium on Naval Hydrodynamics, The National Academies Press, Washington DC, 2004, pp. 270–292.

Chen, B., Stern, F., "Computational Fluid Dynamics of Four- Quadrant Marine-Propulsor Flow," Journal of Ship Research, Vol. 43, No. 4, 1999, pp. 218–228.

Davoudzadeh, F., Taylor, L. K., Zierke, W. C., Dreyer, J. J., McDonald, H., Whitfield, D. L., "Coupled Navier-Stokes and Equations of Motion Simulation of Submarine Maneuvers, Including Crashback," Proceedings of the 1997 ASME Fluids Engineering Division Summer Meeting, Vol. 2, ASME, New York, 1997.

McDonald, H., Whitfield, D., "Self-Propelled Maneuvering Underwater Vehicles," 21st Symposium on Naval Hydrodynamics, The National Academic Press, Washington, DC, 1996, pp. 478–489.

Vyšohlíd, M., Mahesh, K., "Large Eddy Simulation of Propeller Crashback," Flow Induced Unsteady Loads and the Impact on Military Applications, Meeting Proceedings RTO-MP-AVT-123, Neuilly-sur-Seine, France, 2005, pp. 2-1 – 2-12.

Vyšohlíd, M., Mahesh, K., "Large Eddy Simulation of Propeller Crashback," Proceedings of the 44th AIAA Aerospace Sciences Meeting and Exhibit, AIAA, paper 2006-1415.

Beddhu, M., Taylor, L. K., Whitfield, D. L., "Strong Conservative Form of the Incompressible Navier-Stokes Equations in a Rotating Frame with a Solution Procedure," J. of Computational Physics, Vol. 128, 1996, pp. 427–437.

Majety, K. S., "Solutions to the Navier-Stokes Equations in a Non-Inertial Reference Frame," MS Thesis, Mississippi State University, 2003.

Mahesh, K., Constantinescu, G., Moin, P, "A Numerical Method for Large-Eddy Simulation in Complex Geometries," J. of Computational Physics, Vol. 197, No. 1, 2004, 215–240.

Germano, M., Piomelli, U., Moin, P., Cabot, W. H., "A Dynamic Subgrid-Scale Eddy Viscosity Model," Physics of Fluids A, Vol. 3, No. 7, 1991, 1760-1765.

Lilly, D. K., "A Proposed Modification of the Germano Subgrid-Scale Closure Method", Phyics of Fluids A, Vol. 4, No. 3, 1992, 633-635.

Hecker, R., Remmers, K, "Four Quadrant Open-Water Performance of Propellers 3710, 4024, 4086, 4381, 4382, 4383, 4384 and 4426," David Taylor Naval Ship Research and Development Center, report NSRADC 417-H01, 1971.

Carlton, J.S., "Marine Propellers and Propulsion," Butterworth-Heinemann Ltd, Oxford, UK, 1994, pp. 163-165.